Kinetics of Initiation of the Third Generation Grubbs Metathesis Catalyst: Convergent Associative and Dissociative Pathways

Citation for published version:
Forcina, V, Garcia-dominguez, A & Lloyd-jones, GC 2019, 'Kinetics of Initiation of the Third Generation Grubbs Metathesis Catalyst: Convergent Associative and Dissociative Pathways' Faraday Discussions. DOI: 10.1039/C9FD00043G

Digital Object Identifier (DOI):
10.1039/C9FD00043G

Published In:
Faraday Discussions

ARTICLE

Kinetics of Initiation of the Third Generation Grubbs Metathesis Catalyst: Convergent Associative and Dissociative Pathways

Received 00th January 20xx,
Accepted 00th January 20xx

DOI: 10.1039/x0xx00000x

Veronica Forcina,[a] Andrés García-Domínguez[a] and Guy C. Lloyd-Jones*[a]

The kinetics of the nominally irreversible reaction of the third generation Grubbs catalyst G-III-Br (4.6 μM) with ethyl vinyl ether (EVE) in toluene at 5°C have been re-visited. There is a rapid equilibrium between the bipyridyl form of G-III-Br, 1, and its monopyridyl form, 2, ($K \approx 0.001$ M). Empirical rate constants (k_{obs}) for reaction with EVE, determined UV-vis spectrophotometrically under optimised anaerobic stopped-flow conditions, are analysed by testing the quality of fit of a series of steady-state approximations. The kinetics do not correlate with solely dissociative or associative pathways, but do correlate with a mechanism where these pathways converge at an alkene complex primed to undergo metathesis. In the presence of traces of air there is a marked increased in the rate of decay of G-III-Br due to competing oxidation to yield benzaldehyde; a process that appears to be very efficiently catalysed by trace metal contaminants. The *apparent* acceleration of the initiation process may account for the rates determined herein being over an order of magnitude lower than previously estimated

Introduction

Initiation in Metathesis. Over the last two decades, ruthenium alkylidene catalysed alkene metathesis[1] has become ubiquitous, with applications at scales ranging from μg,[2] to kg.[3] Much of this has been the direct consequence of a sustained period of development of a series of robust and well-characterised Ru-complexes,[1] with three general mechanistic events[4] identified as initiation,[5,6] turnover, and decomposition.[7] Initiation and turnover are mechanistically-related, and comprise, *inter alia*, alkene coordination, mutual interconversion of the alkylidene-alkene pair via a ruthenacyclobutane, then dissociation or displacement of the newly formed alkene. The co-product from initiation, most frequently styrene, or a derivative,[8] is non-innocent, able to undergo competitive metathetic reincorporation at ruthenium to regenerate the benzylidene complex.[9]

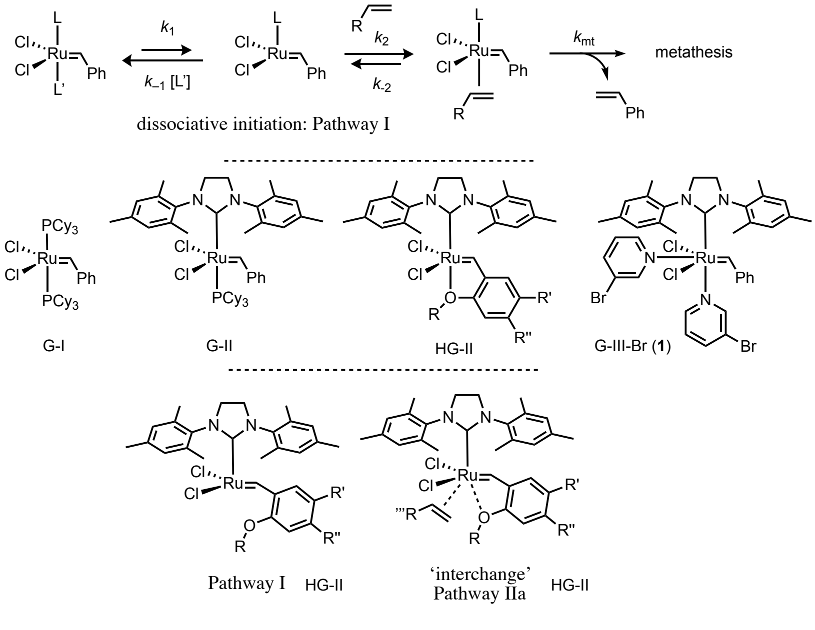

[a] EaStChem, School of Chemistry, Joseph Black Building, David Brewster Road, EH9 3FJ, Edinburgh. guy.lloyd-jones@ed.ac.uk

Figure 1: Generic dissociative (pathway I) initiation mechanism for ruthenium-alkylidene complexes G-I, G-II, and *additional* associative-interchange (pathway IIa) for HG-II.

Exquisite detail regarding catalyst turnover has been elucidated using techniques such heteronuclear NMR magnetisation transfer,[10] dynamic nuclear polarisation labelling,[11] and single-molecule fluorescence.[12] However, much of the work in the primary phases of development of new ruthenium pre-catalysts, and the investigation of their relative efficiency and activity, focussed on the initiation event.[1,4,5] A now classic example of such initiation studies is the series of experiments reported by Grubbs, Sanford and Love, et al. in which a large excess of ethyl vinyl ether (EVE) was used to generate styrene and a stable Fischer-type alkylidene product [Ru]=CHOEt, in an apparently irreversible manner.[14] Using this approach, the kinetics of initiation, of both G-I and G-II, were shown to proceed via pathway I (Figure 1).[14,15]

The initiation mechanisms for a wide variety of other Grubbs type catalysts have been studied, at varying levels of detail, both computationally and experimentally.[5] Most salient to the results presented herein, are the in-depth investigations by Plenio,[16] and Percy,[17] of the initiation of the HG-II catalyst,[18] and analogues.[16] Kinetic data were analysed either by addition of a simple linear correction term, first order in alkene, to the standard hyperbolic fitting function for dissociative pathway I, or by assumption of second-order process.[17] The kinetics,[16] and activation parameters,[17] were indicative that an associative 'interchange' (pathway IIa, Figure 1) can also contribute to initiation.[16,17]

The Grubbs Third Generation Catalysts (G-III-X). In 2001, Grubbs and Love, reported the G-III-X, (X = H, Cl, Br,) catalysts, that undergo exceptionally fast initiation.[19] In preliminary studies by UV-vis spectrophotometry, the lower-limit for the dissociative initiation (k_1) of the fastest catalyst, G-III-Br, was estimated to be >4 s^{-1}; *more than six orders of magnitude* faster than G-II,[14] and three orders of magnitude faster than HG-II.[18] The readily-synthesised third generation system G-III-Br (**1**) remains one of the fastest-initiating commercially available ruthenium alkylidene metathesis catalysts.[1]

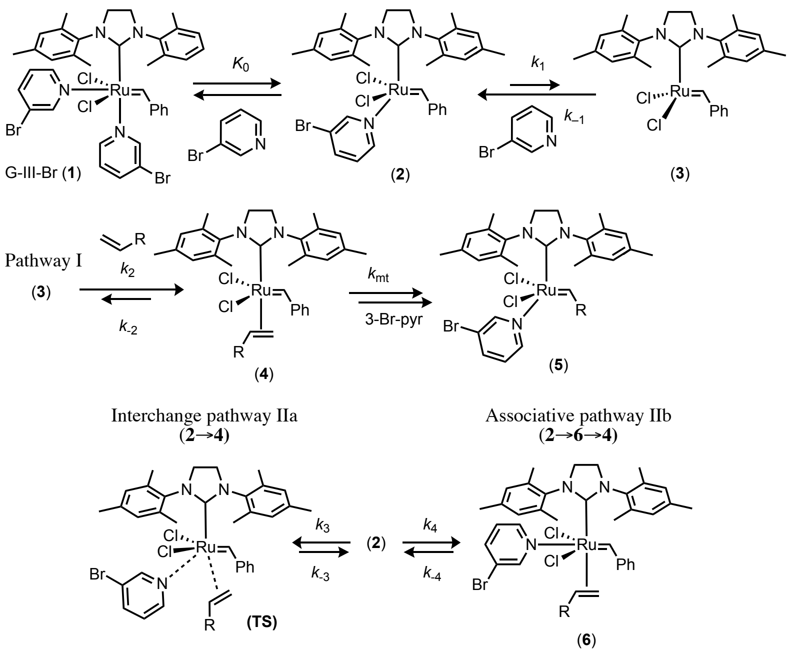

Figure 2: Trzaskowski and Grela's computational analysis[20] of mechanisms for initiation of the third-generation catalyst G-III-Br with ethene (R = H) and butene (R= Et).

In 2013 Trzaskowski and Grela reported a computational analysis of possible metathesis initiation pathways of G-III-X pre-catalysts (X = Br, H) by ethene and but-1-ene, Figure 2.[19] A number of important conclusions were drawn. Firstly, the dissociation of a pyridine ligand from G-III-X (1 M standard state) was predicted to be only slightly endergonic, leading to K_0 values in the range 10^{-3} to10^{-1} M. Secondly, in complex **2**, the remaining pyridine ligand occupies a site that is intermediate between the *cis* and *trans* locations of the two pyridyl ligands in the precursor G-III-Br, **1**. Thirdly, dissociation (k_1) of the remaining pyridine ligand from **2**, to generate the 14e⁻ complex **3**, is also predicted to be only mildly endergonic, with a transition state barrier of between 10.1-13.6 kcal mol^{-1}; subsequent alkene coordination (k_2, to generate complex **4**, Figure 2) has a low barrier (<4 kcal mol^{-1}), and is mildly exergonic. Finally, a pathway involving association (k_3; k_4) of the alkene with monopyridyl complex **2** to generate a discrete 18e⁻ intermediate (analogous complex to **6**, Figure 2), en route to 16e⁻ alkene complex **4**, (stepwise associative, type IIb) was computed to have a similar barrier (at standard state) to dissociation (pathway I) and a lower barrier than direct formation of **3** via interchange (IIa) at the 16e⁻ intermediate **2**,

Figure 2. Thus overall, it was concluded, from DFT energetics, that dissociative (pathway I) and associative-dissociative (pathways IIa,b) processes are all feasible mechanisms to initiation, and simultaneously that they are the rate-limiting steps for the overall initiation process.[20]

In 2017, Guironnet reported detailed NMR studies of the solution phase speciation of G-III-X complexes (X = H, Br), and on the kinetics of polymerisation of *N*-hexyl-*exo*-norbornene-5,6-dicarboximide.[21] Consistent with the calculations of Trzaskowski and Grela,[20] titrations of G-III-X (X = H, Br) in CH_2Cl_2 with pyridine, monitored by ^1H NMR, established that at room temperature, K_0 = 0.4-0.5 M for G-III-H, and 2.4 M for G-III-Br, **1**.[21] Guironnet demonstrated that this has significant phenomenological impact on the metathesis kinetics, notably in living-polymerisation, since the net effect of using G-III-Br **1** is that the pre-dissociated 3-Br-pyridine (L), present at a concentration identical to the active species, **2**, acts as an inhibitor to initiation and then turnover. Grubbs later reported on the co-polymerization kinetics of 23 different norbornenyl comonomers with ω-norbornenyl macromonomer, catalysed by G-III-H, for which ^1H NMR pyridine titrations of G-III-H in CH_2Cl_2 yielded K_0 = 0.25 M, at room temperature.[22] The polymerization kinetics were analysed on the basis of the dissociative mechanism (pathway I) in which a monoligated intermediate [(IMes)Ru(=CH*poly*)Cl_2(3-H-pyr)$_1$] (*poly* = living polymer) is the dominant resting state in a pre-saturation regime ($k_2 << k_{-1}$). However, it was noted that the associative pathway II, proceeding in a stepwise (IIb) or concerted (IIa)[19] manner, could not be conclusively ruled out.[21]

Herein, we revisit the reaction of G-III-Br (**1**) with ethyl vinyl ether (EVE, 'E') in toluene at 5° C, Figure 3,[19] to test whether the dissociative (I) and associative (II) pathways explored computationally by Trzaskowski and Grela,[20] Figure 2, can be distinguished experimentally.[18]

Results and discussion

Initial tests confirmed that the alkylidene Ru=CH signal in the ^1H NMR spectra of (**1**,**2**) and (**5**$_{Et}$) were well resolved in toluene (19.4 ppm versus 13.8 ppm, respectively), and that addition of ≥1.1 equivalents of EVE to (**1**,**2**) led to >99% conversion to **5**$_{Et}$. We began by exploring automated rapid quenched-flow (RQF, Figure 3) using butyl vinyl ether, BVE in large excess (100 equiv.) as quenching agent (*Q*). However, control experiments showed that, somewhat surprisingly, that **5**$_{Et}$/**5**$_{Bu}$ undergo relatively efficient metathesis with BVE and EVE, respectively, leading to erosion of the kinetic trapping ratio of **5**$_{Et}$/**5**$_{Bu}$, over a period of minutes, even after adding PPh_3 as a stabiliser.

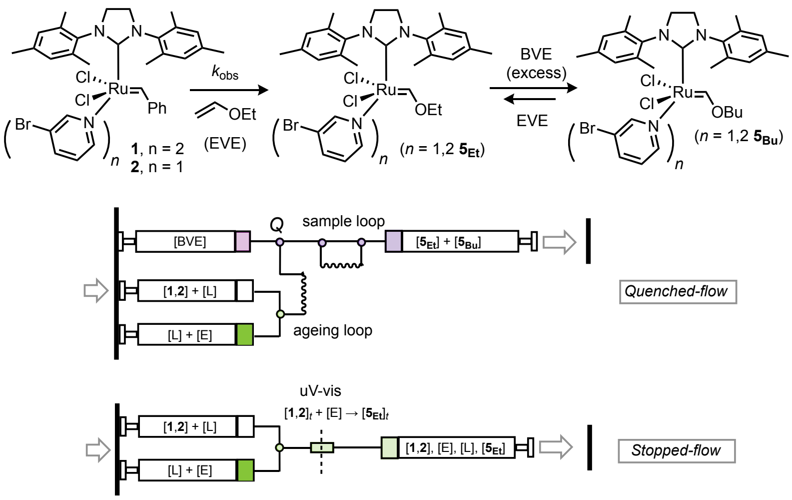

Figure 3: Kinetics of initiation (k_{obs}) of G-III-Br (**1**,**2** + L) with excess ethyl vinyl ether (E, EVE), and schematics of mixing of reactants via rapid quenched-flow (RQF, with excess butyl vinyl ether (BVE) quenching agent, *Q*) and stopped-flow (SF-UV-vis). PPh_3 and PCy_3 proved inefficient as quenching reagents.

Stopped-Flow UV-Vis Analysis. Given the above complications, we turned to analysis of the reactions by in situ UV-Vis spectrophotometric analysis.[19] Using a stopped-flow system, Figure 3, we monitored the signal centred at 354 nm, assumed to arise from metal to benzylidene π* charge transfer analogous to that with H-G-II,[16] and absent in the initiation product ([Ru]=CHOEt), which lacks the conjugated phenyl group. Whilst this *in situ* method leads to a substantial increase in data-density compared to e.g. RQF, the low concentrations of $[Ru]_{tot}$ (approx 50 μM) required for the UV-Vis analysis initially resulted in some variability in rates between runs. This was eventually identified as arising from trace diffusion of air into reagent delivery lines, the solvent-purification system, and into sample reservoirs in the stopped-flow apparatus, which led to periods during which the first-order rate of initiation, based on quenching of the UV absorption at 348 nm, *appeared* to increment between runs. Deliberate oxidation of G-III-Br in d_8-toluene was monitored by ^1H NMR, which confirmed benzaldehyde generation by oxidative cleavage of the benzylidene ligand, and thus loss of the moiety responsible for the 348 nm MLCT band; the complex mixture of ruthenium co-products was not further investigated. Subsequent tests confirmed that the aerobic oxidation reaction of dilute solutions of G-III-Br (**1**,**2**) in toluene solution, as monitored by the decay of the MLCT band at 354 nm, is not photocatalysed (decay rates were unaffected by gating the UV-vis irradiation) but is highly sensitive to the method of stock-solution preparation and its introduction into the stopped-flow system. Passage of the solution of G-III-Br through stainless-steel needles during sample preparation (sequential dilutions etc.) or during introduction to the apparatus, induces very rapid oxidative decay rates, as compared to samples prepared and delivered solely through glass / PTFE systems.‡ After extensive procedural refinement of the overall process, the rates of decay of the MLCT band became stable and reproducible, within experimental error, between samples and runs, including attenuation to zero when no EVE was present, and thus attributable solely to metathesis initiation, rather than other competing processes.

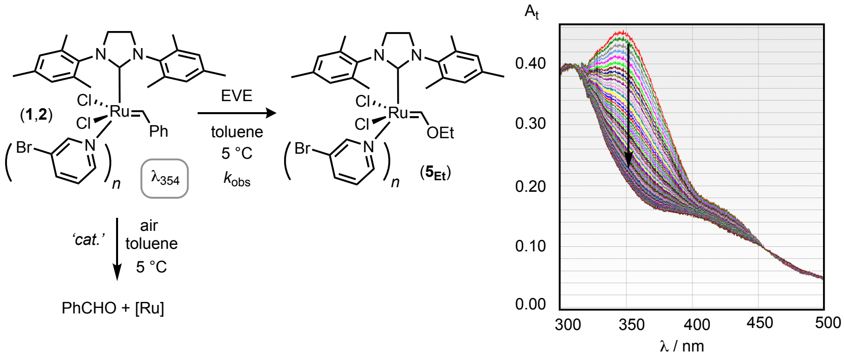

Figure 4: General scheme for kinetics of the initiation (k_{obs}) of G-III-Br (**1**,**2** + L) with excess ethyl vinyl ether (E, EVE), and example series of 200 transient UV spectra, $\Delta t_{n,n+1}$ = 40 msec, obtained on mixing **1**,**2** + L $[Ru]_{tot}$ = $[L]_{tot}$ = 0.046 mM) with ethyl vinyl ether ($[E]_0$ = 0.83 M).

Kinetics of reaction of EVE with G-III-Br. Using the stopped-flow method, kinetic data were obtained from the temporal decay of the signal at 354 nm, Figure 4, obtained approximately 8 msec after mixing of a solution of G-III-Br (**1**,**2**) + 3-Br-pyridine $(Ru]_{tot}$ = 'L' = 92 μM) with solutions of ethyl vinyl ether ('E', 0.8 mM to 1.66 M) in toluene at 5.0±0.1 °C. In further experiments, the solution of ethyl vinyl ether also contained 3-Br-pyridine ('L', 0 to 4.2 mM). Empirical first order rate constants were obtained by non-linear regression of the exponential decay in absorbance, Figure 5. First-order decays in the signal were obtained through >6 half-lives (>98% conversion) under all conditions tested. Empirical rate constants, k_{obs}, Table 1, were then determined by averaging a minimum of 10 experiments per concentration variation. For comparison, analogous experiments were conducted with the slower-initiating G-I catalyst system, at [EVE] concentrations ranging from 0.1 to 1.5 M, again in toluene, but at 21 °C, Table 2

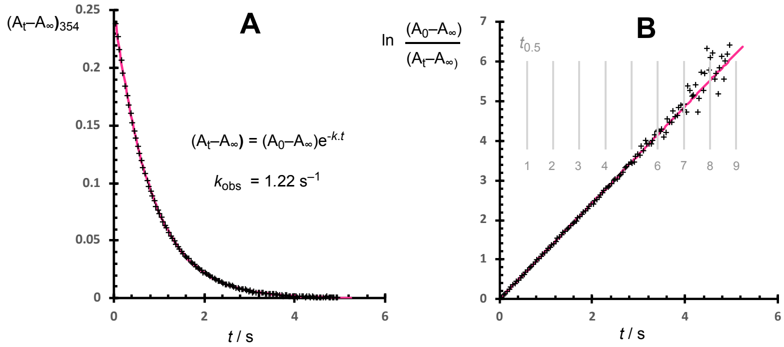

Figure 5: **A**. Example analysis of the kinetics of initiation (k_{obs}) of G-III-Br (**1**,**2** + L) with excess ethyl vinyl ether (E, EVE) in toluene at 5 °C. **A**. Exponential decay of the signal at 354 nm, with non-linear regression, k = 1.22 s^{-1}. **B**: First-order behaviour in decay of **1**,**2** with half-lives indicated.

Table 1. First-order empirical rate constants (k_{obs} / s) for decay of **1**,**2** by reaction with ethyl vinyl ether in toluene at 5 °C, monitored using Stopped-flow UV-Vis.

entry	$[EVE]_0$ /M	$[L]_{added}$ /mM	k_{obs} /s^a
1	0.063	0.000	0.29(0.03)
2	0.310	0.000	0.57(0.03)
3	0.520	0.000	0.90(0.05)
4	0.630	0.000	1.06(0.05)
5	0.690	0.000	1.00(0.02)
6	0.830	0.000	1.26(0.05)
7	0.063	0.250	0.18(0.02)
8	0.310	0.250	0.31(0.02)
9	0.630	0.250	0.50(0.03)
10	0.830	0.250	0.63(0.01)
11	0.063	0.446	0.15(0.01)
12	0.310	0.446	0.24(0.01)
13	0.630	0.446	0.36(0.02)
14	0.830	0.446	0.44(0.007)
15	0.063	1.046	0.10(0.01)
16	0.310	1.046	0.14(0.01)
17	0.630	1.046	0.22(0.01)
18	0.830	1.046	0.24(0.01)
19	0.063	2.050	0.06(0.003)
20	0.310	2.050	0.09(0.007)
21	0.630	2.050	0.12(0.01)
22	0.830	2.050	0.15(0.01)
23	0.0004	0.000	0.06(0.002)
24	0.0020	0.000	0.14(0.01)
25	0.0040	0.000	0.21(0.02)
26	0.0063	0.000	0.22(0.03)
27	0.0340	0.000	0.29(0.03)
28^b	0.063	0.000	0.35(0.05)

^{a}.k_{obs} non-linear regression, see Figure 5; average of ≥20 determinations, with standard deviation for each dataset (1σ) in parenthesis. [Ru]tot = 0.046 mM. Concentrations are after mixing at 5±0.1 °C. ^{b}.Reaction in toluene / Et_2O; (EVE + Et_2O) = 0.83 M.

Table 2. First-order empirical rate constants (k_{obs} / s) for decay of G-I by reaction with ethyl vinyl ether in toluene at 21 °C, monitored using stopped-flow UV-Vis.

entry	$[EVE]_0$ /M	$[L]_{added}$ /mM ^{b}	k_{obs} /s^a
1	0.146	0.000	0.0070(0.0002)
2	0.198	0.000	0.0079(0.0002)
3	0.245	0.000	0.0080(0.0002)
4	0.371	0.000	0.0097(0.0002)
5	0.493	0.000	0.0110(0.0001)
6	0.618	0.000	0.0110(0.0001)
7	0.668	0.000	0.0108(0.0001)
8	0.718	0.000	0.0113(0.0001)
9	0.912	0.000	0.0119(0.0001)
10	1.500	0.000	0.0123(0.0002)

^{a}.k_{obs} is an average of ≥10 experiments, obtained by non-linear regression of growth of the signal at 484 nm. Standard deviation (1σ) in parenthesis. [Ru]tot = 0.046 mM. Concentrations are those after mixing at 21±0.1 °C. ^{b}.No additional ligand was added.

Table 3. Empirical coefficients, *a* and *b*, at various ligand ([L]) concentrations, for the dependence of first-order rate empirical rate constant $k_{obs} = a[E] + b$, for the reaction of G-III-Br with ethyl vinyl ether (E) in the range $[E]_0$ = 0.06 to 0.83 M, toluene, 5 °C.

entry	$[L]_{tot}$ /mM^a	a / $M^{-1}s^{-1}$	b / s^{-1}
1	0.046	1.26	0.21
2	0.296	0.59	0.14
3	0.492	0.36	0.12
4	1.092	0.20	0.08
10	2.096	0.11	0.05

^{a}.$[Ru]_{tot}$ = 0.046 mM. [L] includes endogenous 3-Br-pyridine, calculated using K_0 = 0.001 M. Reactions in toluene at 5±0.1 °C.

As anticipated,[14] the data obtained for the G-I system Table 2) gave a simple correlation with [EVE], as analysed graphically, Figure 6A, by application of the standard steady-state rate equation for pathway I, yielding an initiation rate (k_1) of 0.014±0.002 s^{-1} at 21 °C, in agreement with the value reported by Sanford, Ulman and Grubbs (0.016 s^{-1}).[14]

In contrast to G-I, application of the analogous standard steady-state rate equation for pathway I[14-16] for the data obtained with G-III-Br (Table 1), did not give a simple linear correlation, Figure 6B, indicative that dissociation (k_1) does not dominate initiation across the range of concentrations tested. Reactions conducted without added 3-Br-pyridine (L) and with ethyl vinyl ether (E) concentrations in the range 0.06 to 0.83 M (Table 1, entries 1-6) gave rates that were linearly dependent on [E]; but had a substantial non-zero *y*-axis intercept: $k_{obs} = a[E] + b$; Table 3, entry 1. The kinetics deviated strongly from the relationship $k_{obs} = a[E] + b$ when $[E]_0 \leq 4$ mM (Table 1, entries 23-27); see below for further discussion and global kinetic analysis. Inclusion of exogenous ligand ([L] = 0.3-2 mM, Table 1, entries 7-22) resulted in progressive reduction in the empirical coefficients *a* and *b*, Table 3, entries 2-5. Graphical analysis showed that *both* 1/*a* and 1/*b* have an approximately linear dependence on [L], Figure 6C, indicative of inhibition by added ligand L, via at least two pathways.

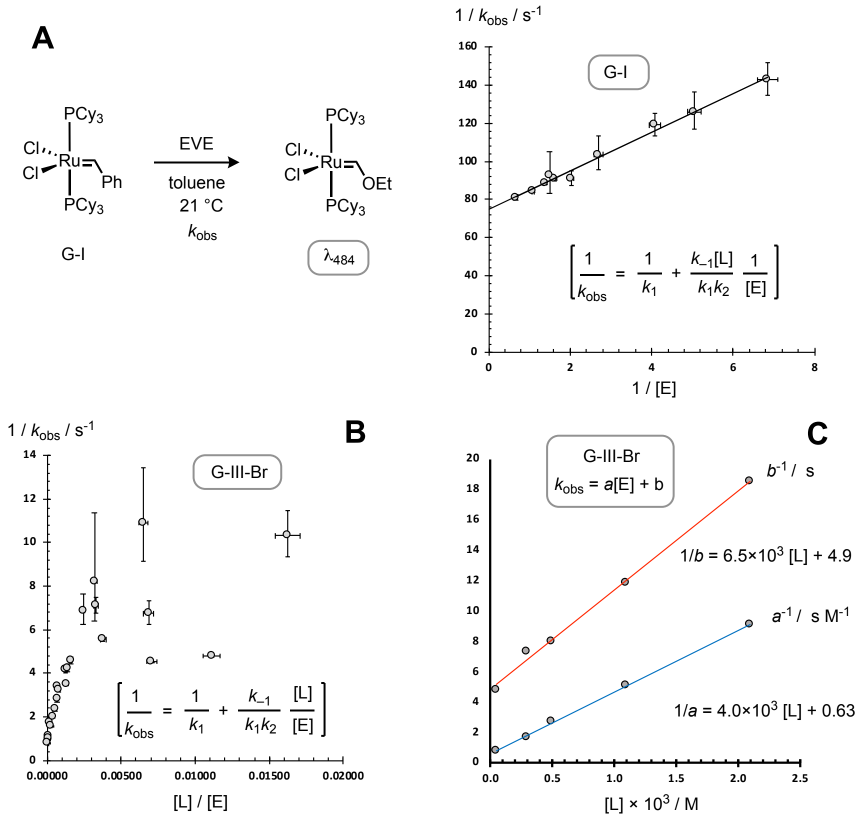

Figure 6: Preliminary analyses of rate-data from Tables 1 and 2, employing equation for initiation *solely* via dissociative pathway I (see Figure 2 for rate constant definitions). **A**: G-I initiation at 21°C; correlation: $1/k_{obs}$ = 10.5/[E] + 74, leads to k_1 = 0.014 s^{-1}. Error bars are propagated from ±1σ in k_{obs} and ±2.5% in [E]. **B**. G-III-Br initiation at 5°C; scattered correlation. Table 1 entries 19 and 23 omitted for clarity. [L] calculated from K_0 = 0.001 M. Error bars are propagated from ±1σ in k_{obs} and ±2.5% in *both* [L] and [E]. **C**. Correlation of empirical coefficients for k_{obs} = *a* [E] + *b*, Table 3, with $[L]_{tot}$, leading to k_{obs} / s = ([E] / (4.0×10³ [L] + 0.63)) + 1 / (6.5×10³ [L] + 4.9), when 0.83 ≥ [E] ≥ 0.06 M and [L] , calculated using K_0 = 0.001 M, is in the range 0.05 to 2.1 mM.

Ligand dissociation from G-III-Br. Guironnet[21] and Grubbs,[22] have independently determined K_0 for G-III-H and G-III-Br in CH_2Cl_2. The values from van't Hoff analysis of G-III-H,[21] together with the (K_0^{Br}/K_0^{H}) ratio of 4.8, might then suggest that for the reactions reported herein there will be >99% dissociation of **1** to **2**. However, this requires there is a negligible impact of solvent (CH_2Cl_2 versus toluene) on the equilibrium. G-III-Br was thus analysed by ^1H NMR in d_8-toluene at 5°C, combining data from a series of additions of 3-bromopyridine ligand to **1**, and a series of dilutions of **1** without added ligand. Linear regression of the time-average population-weighted chemical shift of the benzylidene CH signal (19.3-19.5 ppm) against that calculated using a standard quadratic equation for equilibrium of **1** with **2**, with K_0, δ_1 and δ_2 as variables, Figure 7, established that ligand dissociation from **1** is considerably less favourable in toluene at 5 °C, compared to CH_2Cl_2 at room temperature.

Given the sensitivity of the equilibrium to solvent, the initiation rate of G-III-Br conducted at high concentrations of ethyl vinyl ether, [E], could conceivably be affected by the change in medium from pure toluene to mixtures of toluene and ethyl vinyl ether. A control experiment in which the reaction was conducted in toluene containing 0.063 M ethyl vinyl ether and 0.767 M Et_2O, as a non-metathetic surrogate, gave a similar empirical rate constant to that conducted with just the ethyl vinyl ether in toluene (Table 1, entries 1 and 28), indicative that the changing reaction medium does not contribute significantly to the observed increase in empirical coefficient *a* as [E] is increased.

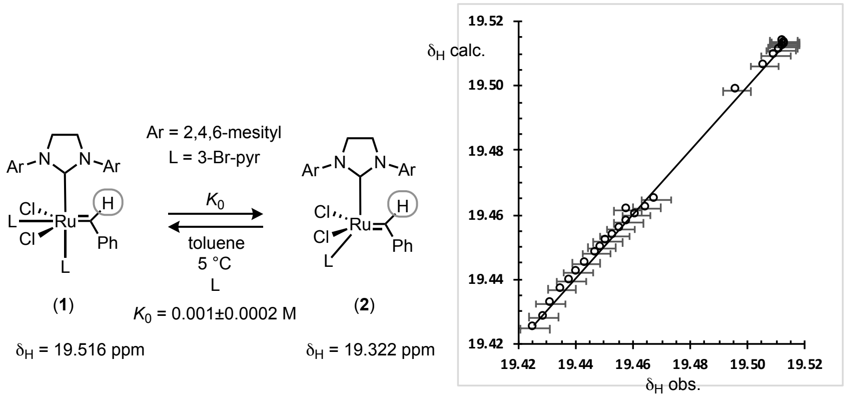

Figure 7: [1]H NMR analysis the chemical shift of the benzylidene-CH in G-III-Br in d_8-toluene at 5°C as a function of concentration of **1** ($[Ru]_{tot}$ = 2.1 to 9.7 mM) and 3-Br-pyridine (8.9-89 mM at $[Ru]_{tot}$ = 8.33 mM). Linear regression of the observed (*x*-axis) time-average population-weighted (**1**+**2**) chemical shift of the benzylidene-CH against that calculated (*y*-axis) when K_0 = 0.001 M, δ_1 = 19.516 ppm and δ_2 = 19.322 ppm, referenced against residual d_7-toluene CHD_2 = 2.128 ppm. Correlation: $\delta_{calc} = 0.9981(\delta_{obs}) + 0.0361$; RMSE, ±0.00005, yielding K_0 = 0.001±0.0002 M. Error bars in δ_{obs} are at 0.005 ppm.

Steady-state analyses of dissociative and associative initiation mechanisms for G-III-Br. A dissociative mechanism beginning from **2**, and proceeding via **3** and **4**, to irreversibly generate **5** will result in the rate of metathesis rising as the ethyl vinyl ether concentration, [E], is raised, but in a decreasingly proportionate manner, eventually reaching an asymptote when $k_2k_m[E] >> k_{-1}[L](k_{-2} + k_m)$, such that the *overall* rate of conversion of **2** to **5** becomes independent of [E] and is dictated solely by the rate of ligand (L) dissociation (k_1); i.e. saturation kinetics. Based on the pyridine dissociation constant (K_0) determined herein (Figure 7) the speciation of the G-III-Br complex **1** in solution under the conditions employed for stopped-flow UV-Vis will vary from being dominated by monopyridyl complex **2** (96%), when no exogenous 3-bromopyridine ligand (L) is present, through to predominantly the bispyridyl complex **1** (66 %) when L = 2 mM. Thus, as the free ligand concentration, [L], is raised (Table 1, entries 7-22) the rate of metathesis will be attenuated in both the pre-saturation phase, and the saturation phase, as outlined schematically in Figure 8A.

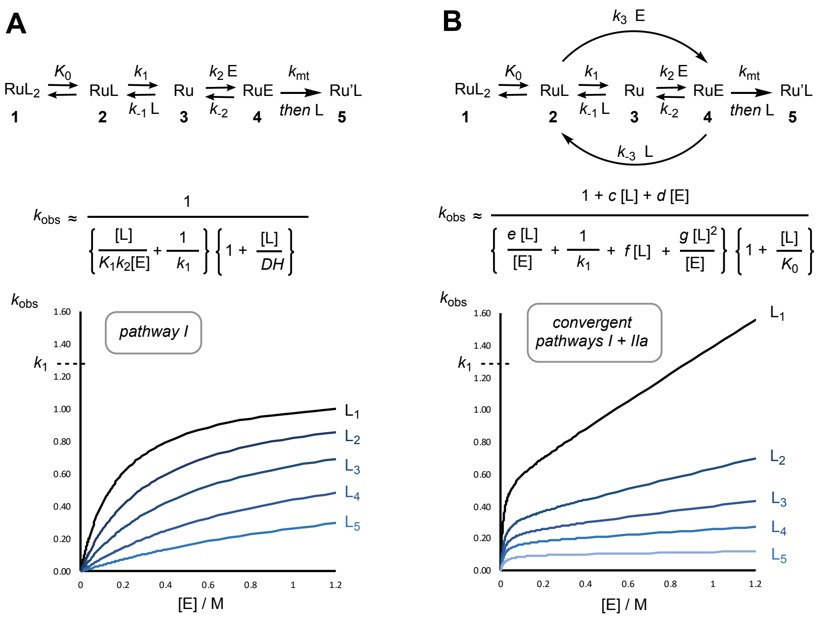

Figure 8: Generic kinetic profiles (arbitrary values; *y*-axis: k_{obs}, *x*-axis: alkene concentration (E)) for initiation of a RuL_2 complex, at various exogenous ligand concentrations (L_{1-5}) *via* a solely dissociative mechanism (Pathway I, **A**) versus a mechanism in which dissociative and associative processes *converge* at alkene complex **4** (Pathways I + IIa; **B**), where $c = k_3/K_1k_2$, $d = k_3/k_1$, $e = (1/K_1K_2k_{mt} + 1/K_1k_2)$, $f = k_{-3}/k_1k_{mt}$, $g = k_{-3}/K_1k_2k_{mt}$. The fast pre-equilibrium K_0 determines the mol fraction [**2**] for the steady-state approximation.

However, even with this adjustment for K_0, the single-pathway dissociative mechanism (pathway I) is inconsistent with the observed dependencies on [E] and [L], Table 1. Augmentation of the steady-state rate equation for pathway I with an additional term that *solely* comprises a divergent associative pathway (IIa or IIb)[16] gives a better, but still imperfect, correlation. However, non-linear regression of the predicted versus empirical rate constant (k_{obs}) as a function of [E] and [L] using a speciation-weighted (K_0) steady-state rate equation in which **2** undergoes conversion to **5** via *convergence* of pathways I and II at intermediate **4** (Figure 8B) gives a good overall correlation, Figure 9A, including data at low concentrations of [E] and [L], where the dominant process is dissociative (pathway I), see inset to Figure 9B. A key component in the steady-state analysis for convergent mechanism I+II is that the dissociative pathway *via* **2**→**3**→**4** can be attenuated by direct conversion of **4** to **2**, (or **6**), by [L], which phenomenologically appears to attenuate the saturation limit (k_1 = 0.24(±0.08) s^{-1} in toluene at 5 °C).

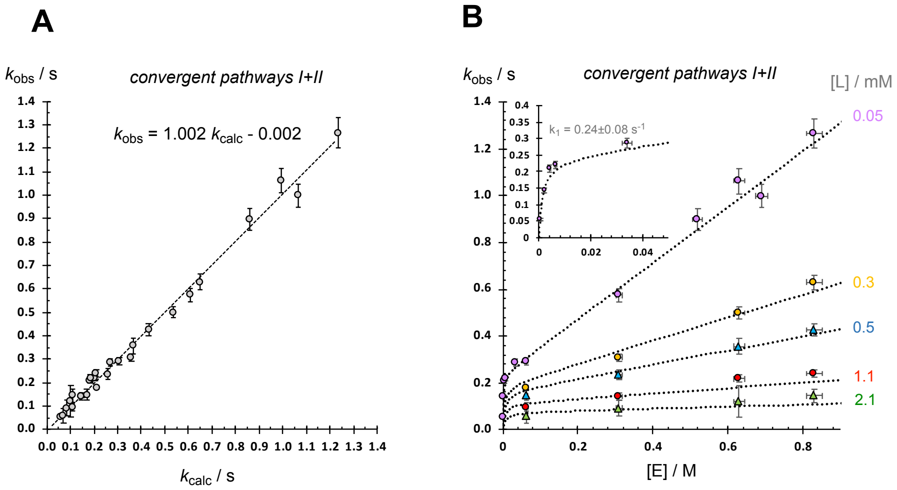

Figure 9: Analysis using steady-state rate equation for convergent mechanism I+II (Figure 8B) and data from Table 1. k_{calc} = x_2 {(1 + 7×10^3 [L] + 6.1[E]) / (1.2×10^2 [L]/[E] + 2.7×10^4[L] + 5×10^5 [L]^2/E + 4.2)}; see Figure 8B. **A**: Correlation of k_{obs} with k_{calc}; R^2 = 0.991. Error bars are plotted at the greater of 5 % / standard deviation (±2σ) for k_{obs}. **B**: Correlations of k_{obs} with [E] (0.0004 to 0.83 M) at various free ligand L concentrations, as indicated. Error bars are plotted at the greater of 5 % / standard deviation (±2σ) for k_{obs}, and ±2.5% for [E]. Dotted lines = k_{calc}. Inset shows region where pathway (I) dominates. In the calculations, x_2 is the mole fraction [**2**]/[Ru] and [L] = [**2**] + [L}$_{exog}$. Both are calculated using a standard quadratic equation for the equilibrium between **1** and **2**, based on K_0 = 0.001 M; see Figure 11, equations 6-8.

Conclusions

The kinetics of the nominally irreversible reaction of the third generation Grubbs catalyst G-III-Br with ethyl vinyl ether (E) in toluene at 5°C have been re-visited.[19] The rapid equilibrium between the bipyridyl form of G-III-Br, **1**, and the monopyridyl form, **2**, was analysed by ^{1}H NMR titration/dilution, yielding K_0 = 0.001 M. Empirical pseudo first-order rate constants (k_{obs}) for the kinetics of reaction of G-III-Br (46 μM) with ethyl vinyl ether (E), to generate **5**$_{Et}$, have been determined under anaerobic stopped-flow conditions by UV-vis spectrophotometric analysis of the decay in of the MLCT band at 354 nM. Across the range of concentrations of exogenous ligand, [L], explored, the speciation of G-III-Br, ranges from 33% to 96 % **2**, based on K_0 = 0.001 M. There was no evidence for any significant accumulation of intermediates, decays in [**1**,**2**] were clean first-order, and isosbestic points in the UV-vis spectra were retained. The empirical rate constants obtained (k_{obs}) were analysed in detail by testing the quality of fit of a series of steady-state approximations. The kinetics correlate with a mechanism where dissociative and associative pathways converge at pyridyl-free complex **4** in which the alkene is bound and is primed to undergo metathesis with the benzylidene. The analysis (Figures 8 and 9) requires that complex **4** has a *lifetime*, and thus k_{mt} < (k_{-3}[L] + k_{-2}), i.e. **4** can revert to both **2** and **3**, or progress to **5**.

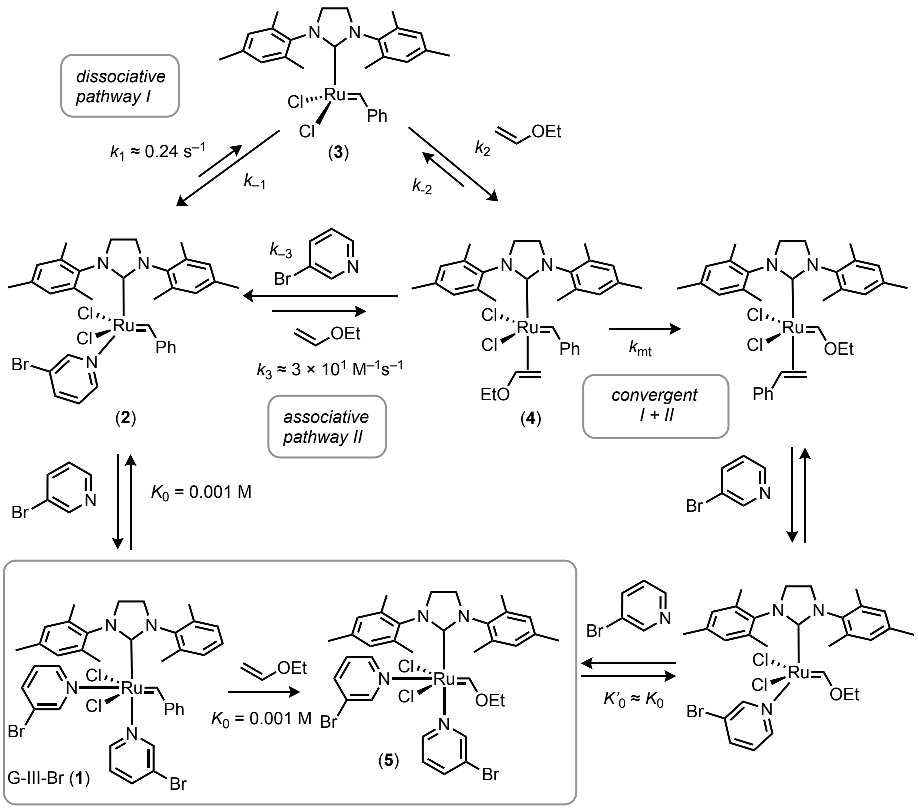

Figure 10: Summary of overall scheme for reaction of G-III-Br with EVE at 5 °C in toluene, and minimal kinetic model for satisfactory simulation (see Figures 8 and 9)

Previous analyses of initiation kinetics for the Grubbs catalysts, and related species, have predominantly, but not exclusively,[16,17] been by application of a steady-state dissociative mechanism (pathway I).[14-22] However, our study strongly supports the conclusions of Trzaskowski and Grela[20] that both the associative and dissociative pathways are kinetically relevant in the initiation, and thus also propagation, of G-III systems. Indeed, the higher the alkene concentration, the more dominant the associative pathway, Figure 10. In principle, saturation kinetics can be achieved for G-III-Br at high alkene [E] concentrations and low ligand [L] concentrations, where the steady-state approximation *for growth of metathesis product* **5** eventually reduces to $k_{obs} \approx k_{mt}$ (IIa and IIb) or k_4 (IIb), accompanied by a change in speciation from (**1**,**2**) to **4** (or alkene complex **6**, Figure 2). However, even when the ethyl vinyl ether concentration approaches its limiting value (≈10.5 M), such saturation may be unachievable. Nonetheless, by using more reactive alkenes, other solvents and at other temperatures, it may be feasible to deconvolute the interchange (IIa) from the step-wise (IIb) association-dissociation pathways for G-III-Br.

Also of interest is the increased rate of decay of the UV-vis signal from the MLCT band in **1**/**2**, arising by competing oxidation to yield benzaldehyde; a process that appears to be catalysed by trace-metal contaminants.[23]‡ Attempts to deliberately induce this effect met with limited success due unreproducible kinetics and very transient periods of stability of [**1**,**2**] prior to decomposition.[24] Nonetheless, the *apparent* acceleration of benzylidene metathesis, (catalysed) oxidation may account for the initiation rate determined herein by stopped-flow UV-Vis herein, being at least an order of magnitude lower[§] than that previously estimated by manual reaction assembly.[19]

Overall, in the context of optimising application of the G-III-Br system in catalysis, for a given level of aerobic exposure, conducting reactions at high catalyst and alkene concentrations will favour turnover over oxidative degradation. Moreover, if other alkenes also propagate by the associative pathway, then the selectivity between competing alkenes may not be a simple linear correlation against their relative concentrations, a factor that may be important in e.g. co-polymerisations.

Experimental

General. All reagents were obtained from Sigma Aldrich. Anhydrous organic solvents were obtained from a solvent purification system (MBraun SPS 800) and dispensed using gas-tight syringes under a positive pressure of nitrogen. NMR spectra were recorded at 27 °C on Bruker Ascend 400 spectrometer. ^{1}H and $^{13}C\{^{1}H\}$ spectra were referenced to TMS. Commercial samples of complex 1 (G-III-Br) were found to be of variable quality. For reproducible kinetic data, the complex was prepared from G-II employing the procedure of Grubbs and co-workers.[18] Thus, G-II (0.5 g, 0.6 mmol) and 3-bromopyridine (1.1 mL, 11.0 mmol) were added to a 20 mL vial. The vial was capped and the reaction mixture was left stirring for 5 minutes while the color changed from red to bright green. Pentane (20 mL) was layered onto the green solution at room temperature to initiate precipitation of a green solid. The vial was then capped and left at −20 °C overnight (freezer). The green precipitate was collected by vacuum-filtration and washed with 4×10.0 mL of room temperature pentane. After drying the precipitate under vacuum, complex 1 was obtained as a green powder (0.4 g, 80% yield) matching all reported spectral data.[18]

Kinetic Analyses. Stopped-Flow UV-Vis experiments were carried out with a Hi-Tech Scientific SFA-20 accessory coupled through a thermostatted umbilical to a Hellma Analytics fused-silica flow cell (5.0±0.1 °C, 80 μL volume, with 10 / 2 mm light paths, and integral mixer), and the outlet connected via the umbilical to a trigger-syringe with microswitch. Within an N_2-filled glovebox stock solutions of G-III-Br (92 mM) and ethyl vinyl ether (0.0008 to 1.66 M; plus 3-bromopyridine 0–4 mM) in toluene were prepared in volumetric glassware, then transferred to 10 mL gas-tight syringes (VWR) coupled to a 1mm OD Tefzel tube and sealed with a plugged flangeless PTFE nut. Prior to kinetic experiments the system was washed through with large volumes of toluene, and then a background UV-vis spectrum recorded. Reagents were then loaded into the two independent 2.5 mL syringe reservoirs via three-way PTFE valves on the SFA-20 connected to the 10 mL gas tight syringes via flangeless fittings, and using hydraulic overpressure for all liquid transfers, i.e. 'pushing' rather than 'pulling' solutions. The system was then flushed twice the stock solutions (5 ml of each, in parallel) to ensure complete purging of toluene, before reloading the reservoirs and conducting a series of 10-25 shots, each comprising 0.1mL of each stock solution. Shots were initiated by a pneumatic drive at constant 5 bar pressure. UV spectra were recorded on Ocean-Optics USB4000 and Flame Spectrometers connected via the cuvette holder to a DH2000-BALUV lamp using solarised resistant grade optical fibres. Data collection was timed by the microswitch on the terminus of the trigger syringe transit, sending a stabilised 5V signal to the spectrometer and PC. 200 UV-vis spectra were recorded over 8 – 80s, depending on k_{obs}, after a deadtime of approximately 8 msec, with a 284-890 nm spectral window. The UV-vis spectra were analysed with Kinetic Studio software, version 5.02, using singular value decomposition (SVD) and recombination of the first two or three components to filter noise. For G-III, rates of reaction (k_{obs}) were obtained by non-linear regression of the exponential decay of the signal (A_t) at 354 nm, averaged across a 0.6 nm spectral range (3 data points) from A_0 to A_∞. Data for G-I, were obtained analogously, but by non-linear regression of the growth of the signal (A_t) at484 nm.

Steady-state rate approximations. Rate equations for Pathway 1, Pathway II, and Pathways I+II were derived using standard Bodenstein approximations to solve for the mol-fraction of pre-metathesis complex **4**, as a function of **2**, assuming that the ruthenium species **2**, accumulating product **5** (in mono and bis-pyridyl forms) and bispyridyl complex **1**, are dominant over all other complexes. Fitting of equation 6 (Figure 11) against the observed data (Table 1) was conducted by non-linear regression of $k_{calc.}$ against $k_{obs.}$ using the Excel solver function to minimise the weighted sum square error, SSE = $\Sigma\{(k_{calc.}–k_{obs.})^2/k_{obs.}\}$. with c, d, e, f, g, and k_1 as variables. Although inclusion of g in the fitting gives a marginally better correlation the model is relatively insensitive to $g \leq 5\ 10^5$. A standard quadratic analysis of the mono / bis-pyridyl speciation from rapid equilibrium (K_0) between **1+5** and **2**, as dictated by $[Ru]_{tot}$ and free [L], was used to correct the rates for mol fraction **2** (x_2, see equation 7, Figure 11). Speciation for mono and bis-pyridyl forms of product **5** was assumed to be similar, i.e. $K'_0 \approx K_0$, and thus free $[L]_{tot}$ is constant through reaction.

$$k_{obs} \approx x_2\, k_{mt}[\mathbf{4}] / [\mathbf{2}]; \quad \text{where } x_2 = [\mathbf{2}]/[\mathrm{Ru}] \qquad (1)$$

$$[\mathbf{4}] \approx \frac{k_2[\mathbf{3}][\mathrm{E}] + k_3[\mathbf{2}][\mathrm{E}]}{k_{-2} + k_{-3}[\mathrm{L}] + k_{mt}} \qquad (2)$$

$$[\mathbf{3}] \approx \frac{k_1[\mathbf{2}] + k_{-2}[\mathbf{4}]}{k_{-1}[\mathrm{L}] + k_2[\mathrm{E}]} \qquad (3)$$

substitution of (eqn 3) into (eqn 2) and rearrangment:

$$[\mathbf{4}] \approx \frac{[\mathbf{2}]\,(k_1k_2[\mathrm{E}] + k_{-1}k_3[\mathrm{L}][\mathrm{E}] + k_2k_3[\mathrm{E}]^2)}{k_{-1}k_{-2}[\mathrm{L}] + k_{-1}k_{-3}[\mathrm{L}]^2 + k_2k_{-3}[\mathrm{L}][\mathrm{E}] + k_{-1}k_{mt}[\mathrm{L}] + k_2k_{mt}[\mathrm{E}]} \qquad (4)$$

substitution of (eqn 4) into (eqn 1) and rearrangment:

$$k_{obs} \approx x_2 \frac{1 + \dfrac{k_{-1}k_3[\mathrm{L}]}{k_1k_2} + \dfrac{k_3[\mathrm{E}]}{k_1}}{\dfrac{[\mathrm{L}]}{K_1K_2k_{mt}[\mathrm{E}]} + \dfrac{k_{-1}k_{-3}[\mathrm{L}]^2}{k_1k_2k_{mt}[\mathrm{E}]} + \dfrac{k_{-3}[\mathrm{L}]}{k_1k_{mt}} + \dfrac{[\mathrm{L}]}{k_2K_1[\mathrm{E}]} + \dfrac{1}{k_1}} \qquad (5)$$

simplifying with coefficients:

$$k_{obs} \approx x_2 \frac{1 + c\,[\mathrm{L}] + d\,[\mathrm{E}]}{e\,[\mathrm{L}]/[\mathrm{E}] + f\,[\mathrm{L}] + g\,[\mathrm{L}]^2[\mathrm{E}] + 1/k_1} \qquad (6)$$

$$[\mathrm{L}] = [\mathbf{2}] + [\mathrm{L}]_{exog.} \qquad (7)$$

solving for [**2**]:

$$[\mathbf{2}] = 0.5 \times \left(\sqrt{([\mathrm{L}]_{exog.} + K_0)^2 - (4\,[\mathrm{Ru}]\,K_0)} - ([\mathrm{L}]_{exog.} + K_0)\right) \qquad (8)$$

when $[\mathrm{L}]_{exog.} >> [\mathrm{Ru}]$

$$x_2 \approx \frac{1}{1 + ([\mathrm{L}]_{exog.} / K_0)} \qquad (9)$$

Figure 11: Derivation of steady-state approximation for initiation mechanism in which dissociative and interchange pathways (I and IIa) converge at intermediate **4**, in which **4** has a discreet lifetime and can revert to starting materials or proceed to metathesis (k_{mt}). An analogous analysis for dissociative and associative pathways (I and IIb) affords essentially the same simplified rate expression as in equation 6, except that (1+*h*) replaces (1) in the numerator.

Conflicts of interest

There are no conflicts to declare.

Acknowledgements

The research leading to these results received funding from the European Research Council under the European Union's Seventh Framework Programme (FP7/2007–2013)/ERC Grant Agreement 340163, the University of Edinburgh (V. F.) and the Swiss National Science Foundation (A.G.D.). We thank Edward J. King (TgK Scientific) for extensive technical advice and assistance.

Notes and references

‡ There was no impact from the use of glass-bodied syringes with PTFE-tipped plungers, versus disposable plastic syringes, versus ground-glass barrel / plunger type syringes. The stainless-steel needles employed for the work are brazed or compression-bonded to a nickel-plated brass Luer-lock hub. The possibility that the 3-Br-pyridine ligand leaches traces of metal from the inside surface of the needle bore (e.g. Ni, Fe, Mn, Cr, Mo) or Luer-lock hub (e.g. Ni, Cu, Zn) is consistent with the observations; there was substantial variability, in terms of impact on the rate of oxidation, between nominally identical needles that were tested. We are currently investigating this phenomenon in more detail, including testing homogeneous solutions of simple pyridyl complexes of a range of transition metals as catalysts for the aerobic oxidation of G-III-Br.

§ The original report (see SI to ref. 19) indicated that on addition of a solution of G-III-Br in toluene to a solution of EVE in toluene in a cuvette at 5 °C, $(\mathrm{Ru})_{tot}$ = 0.046 mM, EVE 17 mM) the UV signal at 354 nM was quenched in less than 0.5 seconds, leading to a dissociative initiation rate (k_{init}) of G-III-Br being estimated as >4 s^{-1}. The rate of reaction of G-III-Br with EVE determined by stopped-flow under the same final concentrations ($[\mathrm{Ru}]_{tot}$ = 0.046 mM, EVE 17 mM) is 0.14 s^{-1}; Figure 9; see also Table 1, entry 24; EVE = 20 mM.

1. For a recent review on advances in ruthenium alkylidene catalysed alkene metathesis, see: O. M. Ogba, N. C. Warner, D. J. O'Leary, R. H. Grubbs, *Chem. Soc. Rev.*, 2018, **47**, 4510–4544.
2. M. Jeschek, R. Reuter, T. Heinisch, C. Trindler, J. Klehr, S. Panke, T. R. Ward, *Nature*, 2018, **537**, 661–668.
3. For examples of the use of transition metal catalysed alkene metathesis in industrial settings see: D. Stoianova, A. Johns, R. Pederson, *Handbook of Metathesis*, Vol 1, Second Edition, Ed. R. H. Grubbs, A. G. Wenzel, Wiley-VCH Verlag GmbH & Co. KGaA, 2015, pp. 699–726. See also reference 1.
4. For an overview of mechanistic events in Ru-catalysed metathesis, see: D. J. Nelson, S. Manzini, C. A. Urbina-Blanco, S. P. Nolan, *Chem. Commun*., 2014, **50**, 10355–10375.
5. For an excellent review on initiation in Ru-catalysed metathesis, see: J. R. Griffiths, S. D. Diver, *Handbook of Metathesis*, Vol 1, Second Edition, Ed. R. H. Grubbs, A. G. Wenzel, Wiley-VCH Verlag GmbH & Co. KGaA, 2015, pp. 273–303.
6. For an example of circumventing poor initiation rate in polymerisation, see J. C. Foster, S. Varlas, L. D. Blackman, L. A. Arkinstall, R. K. O'Reilly, *Angew. Chem. Int. Ed*. 2018, **57**, 10672 –10676, and references therein.

Please do not adjust margins

7 For recent examples of inhibition, see: G. A. Bailey, M. Foscato, C. S. Higman, C. S. Day, V. R. Jensen, D. E. Fogg, *J. Am. Chem. Soc.* 2018, **140**, 6931−6944, and references therein.
8 J. S. Kingsbury, J. P. A. Harrity, P. J. Bonitatebus, A. H. Hoveyda, J. *Am. Chem. Soc.* 1999, **121**, 791-799.
9 For an example of a 'boomerang' system, see: J. M. Bates, J. A. M. Lummiss, G. A. Bailey, D. E. Fogg, *ACS Catal*. 2014, **4**, 2387−2394, and references therein.
10 See e.g. J. A. Love, M. S. Sanford, M. W. Day, R. H. Grubbs, *J. Am. Chem. Soc.,* 2003, **125**, 10103–10109.
11 Y. Kim, C.-H. Chen, C. Hilty, *Chem. Commun.,* 2018, **54**, 4333–4336.
12 Q. T. Easter, S. A. Blum, *Angew. Chem. Int. Ed*. 2018, **57**, 12027–12032.
13 Y. Minenkov, G. Occhipinti, V. R. Jensen, *Organometallics* 2013, **32**, 2099−2111.
14 M. S. Sanford, M. Ulman, R. H. Grubbs, *J. Am. Chem. Soc*. 2001, **123**, 749–750.
15 E. L. Dias, S. T. Nguyen, R. H. Grubbs, *J. Am. Chem. Soc.* 1997, **119**, 3887–3897.
16 V. Thiel, M. Hendann, K.-J. Wannowius, H. Plenio, *J. Am. Chem. Soc*. 2012, **134**, 1104−1114.
17 I. W. Ashworth, I. H. Hillier, D. J. Nelson, J. M. Percy, M. A. Vincent, *Chem. Commun.* 2011, **47**, 5428–5430.
18 S. B. Garber, J. S. Kingsbury, B. L. Gray, A. H. Hoveyda, *J. Am. Chem. Soc.,* 2000, **122**, 8168–8179.
19 J. A. Love, J. P. Morgan, T. M. Trnka, R. H. Grubbs, *Angew. Chem. Int. Ed*. 2002, **41**, 4035–4037.
20 B. Trzaskowski, K. Grela, *Organometallics* 2013, **32**, 3625−3630.
21 D. J. Walsh, S. H. Lau, M. G. Hyatt, D. Guironnet, *J. Am. Chem. Soc*. 2017, **139**, 13644−13647.
22 A. B. Chang, T.-P. Lin, N. B. Thompson, S.-X. Luo, A. L. Liberman-Martin, H.-Y. Chen, B. Lee, R. H. Grubbs, *J. Am. Chem. Soc*. 2017, **139**, 17683−17693.
23 I. Thomé, A. Nijs, C. Bolm. *Chem Soc Rev.* 2012, **41**, 979–987.
24 S. Guidone, O. Songis, F. Nahra, C. S. J. Cazin, *ACS Catal*. 2015, **5**, 2697−2701.